BNL--35549

DE85 006551

SYSTEMATICS ASSOCIATED WITH POSITRONIUM FRACTIONS AS MEASURED WITH VARIABLE-ENERGY POSITRON BEAMS

Peter J. Schultz
Dept. of Phys., Univ. of Western Ontario, London, Ontario, Canada N6A 3K71

K. G. Lynn
Physics Dept., Brookhaven National Laboratory, Upton, New York 11973 USA

H. H. Jorch
Atomic Energy of Canada Ltd. Research Co., Chalk River Nuclear Laboratories
Chalk River, Ontario, Canada K0J 1J0

November 1984

DISCLAIMER

Systematics Associated with Positronium Fractions as Measured with Variable-Energy Positron Beams

Peter J. Schultz* and Kelvin G. Lynn
Brookhaven National Laboratory, Upton, New York 11973

Harald H. Jorch
Atomic Energy of Canada Ltd. Research Co.
Chalk River Nuclear Laboratories, Chalk River, Ontario, Canada K0J 1J0

* Dept. of Physics, University of Western Ontario, London, Ontario, Canada N6A 3K7

Abstract

Positronium fraction measurements using positron beams have been utilized to extract information about the diffusion properties of positrons as well as defect concentrations in the near surface region of materials under a variety of experimental conditions. Owing to this recent interest we have undertaken to study some of the systematics and uncertainties associated with measurements of the positronium fraction, f. We restrict our discussion to determinations of f based on the peak:total ratio of counting rates for a single detector, only briefly considering alternate ways of obtaining f. We conclude with several recommendations that should be of particular interest to practitioners in the field.

I. Introduction

The development of a positron beam for use as a probe of surface and near-surface phenomena ($<10^4$ Å) awaited the discovery of a method to produce a high flux of mono-energetic positrons with variable energy.[1,2] Immediately after this discovery it was determined that a significant fraction of the low-energy positrons that impinge on the surface of the sample leave as positronium (Ps).[3,4] The probability of Ps formation at a surface has now been studied under a variety of experimental conditions as a function of sample temperature, surface conditions, near-surface defect concentration and energy and angle of the incident positron. Fundamentally these kinds of experiments can contribute toward the characterization of the sample's surface condition, although at present the positron behavior, even at "well-characterized" surfaces, is not completely understood.

Studies of Ps have been pursued for more than 30 years. Ore and Powell[5] first predicted the 3-photon decay of the triplet ortho-Ps in 1949, presenting what is currently accepted as the energy distribution of annihilation γ-rays. The existence of ortho-Ps was soon confirmed experimentally by Deutsch,[6] and shortly thereafter Hughes et al.[7] introduced a simple approach to the analysis of the data which has been adapted to the present experimental conditions as follows.

Let N be the number of positron annihilation events occurring in a unit of time. The fraction of these that are due to positrons bound to electrons (Ps) is f and the ortho-Ps to total Ps ratio is denoted by K. Then the annihilations are the sum of the three contributions:

unbound positrons $N_a = N(1-f)$ (1)

para-Ps $N_p = Nf(1-K)$ (2)

ortho-Ps $N_o = NfK$ (3)

Allowing for detection properties like efficiency and resolution of the spectrometer, the solid angle subtended by the detector, the spatial distribution of annihilation events, and γ-ray degradation effects, the counting rate in the photopeak region of the spectrum is

$$P = N[(1-f)g_a + f(1-K)g_p + fKg_o] \quad (4)$$

where g_a is the probability that a photon from an unbound-positron annihilation event will produce a count in the peak region of the spectrum. The probability factors g_p and g_o are defined similarly for para-Ps and ortho-Ps annihilation events. Using h_a, h_p, and h_o, the counts in the total spectrum are

$$T = N(1-f)h_a + Nf(1-K)h_p + NfKh_o \quad (5)$$

Since the detection probability for annihilation events from unbound positrons and para-Ps is virtually identical in most solid state spectrometers,

$$g_a = g_p \quad \text{and} \quad h_a = h_p \quad (6)$$

In the extremes of 100% (f = 1) and 0% Ps formation (f = 0), the count rates are

$$P_1 = N_1[(1-K_1)g_p + K_1g_o] \quad (7)$$

$$T_1 = N_1[(1-K_1)h_p + K_1h_o] \quad (8)$$

and

$$P_0 = N_0g_p \quad (9)$$

$$T_0 = N_0 h_p \tag{10}$$

Now, to remove the count rate dependence at each point, the ratios

$$R = \frac{T-P}{P}, \quad R_1 = \frac{T_1-P_1}{P_1}, \quad R_0 = \frac{T_0-P_0}{P_0} \tag{11}$$

are formed and used along with (6-10) to solve for f in (4) and (5), viz:

$$f = \left[\frac{R_1\left(1-\frac{K}{K_1}\right)+\left(\frac{KR}{K_1}\right)-R_0}{R-R_0} + \frac{K}{K_1}\frac{P_1}{P_0}\frac{N_0}{N_1}\left(\frac{R_1-R}{R-R_0}\right)\right]^{-1} \tag{12}$$

By assuming constant beam current ($N_0 = N_1$) and constant ortho-Ps fraction ($K = K_1$), we can simplify (12) to give the expression:

$$f = \left[1 + \frac{P_1}{P_0}\left(\frac{R_1-R}{R-R_0}\right)\right]^{-1} \tag{13}$$

Although Eq. (13) is the expression typically used[3,4] to calculate f from the annihilation spectrum, it should be emphasized that the underlying assumption of constant beam current ($N_0 = N_1$) may be violated under some experimental conditions. This is discussed in section III. Equation 13 has its obvious counterpart for counts in the valley region, which has often been used interchangeably. The existence of a "100% Ps" state in the slow-positron surface studies of references 3 and 4 is difficult to determine accurately. In addition, the "0% Ps" state is normally found by extrapolation with ≈90% confidence. It is the purpose of this paper to study the validity of this analysis, specifically as related to Eq. (13), and to investigate the consequences of errors in determining the reference states for 0% and 100% Ps.

We organize the discussion under the following sub-headings:

Section II: discussion of some experimental considerations affecting R (eq. 11).

Section III: positron backscattering

Section IV: the effect of the ratio P_1/P_0 on eq. (13).

Section V: derivation of the statistical precision of eq. (13).

Section VI: data simulation to study errors introduced in the 0% and 100% Ps references.

Section VII: the calculation of positron diffusion length using both Ps fraction, f, and annihilation lineshapes, S, is briefly discussed.

Section VIII: discussion of the "red" shift due to Ps fraction and kinetic energy.

Section IX: other methods for determining f.

Section X: summary and recommendations.

II. Experimental Determination of R

The measured parameter R (which is basically the ratio of total:peak counts—eq. 11) is the basis of the calculation of f (eq. 13). There are several factors which contribute to its value, such as the detection system used for the measurement, geometrical arrangement and scattering properties of the apparatus, only electronics (eg. pile-up, summing, very serious resolution degradiation). It is clearly desirable to understand the relationship of each of these to the measured annihilation energy distribution, since the accuracy with which f can be determined depends on the consistency of experimental conditions throughout determinations of R_1, R_0 and the measured variable R.

The energy spectrometers commonly used for measuring the annihilation γ-ray spectra range from Ge(Li) or intrinsic Ge detectors (with resolution of ≈1 to 2 keV FWHM at 511 keV) through to NaI(Tl) scintillation counters on light pipes (with resolution in excess of 100 keV FWHM at 511 keV). The relatively poor efficiency of the semiconductor detectors (<1/3 that of NaI) is thought to be compensated by the ease in clearly demarking the full-energy peak of the spectrum. Failure to completely encompass the peak leads to errors in the total:peak ratio due to instrumental drifts, statistical scatter (see Sec. V and VI), and countrate-related problems such as pulse pileup and incomplete charge collection. Significant improvements may be realized with the utilization of new fast but efficient scintillators (such as BaF_2) coupled to channel-plate photomultipliers (which are not affected by the magnetic field associated with magnetically guided positron beams[8]), however such detection systems have not as yet been tested in this type of experiment.

A problem in measuring R is associated with the scattering of the annihilation radiation in the experimental apparatus. An example of possible arrangements of sample, manipulator, vacuum system and detector is shown in Fig. 1, where the detector is located either to the side or the rear of the sample with respect to the incident positron beam. We shall initially restrict the discussion to the case of a rear-positioned detector, following with a comparison of the two options.

The unbound positrons which annihilate in the sample are typically in the "top" 1000 Å or so, and any Ps which is emitted (the species of interest) is travelling away from the detector. The annihilation radiation that is detected must escape through the combined absorbers of

sample, manipulator, vacuum chamber, water jacket and detector housing. Figure 2 shows a typical spectrum obtained from the Brookhaven apparatus[8] using a Ge(Li) detector, with a Cd single crystal (≈1/4" thick) mounted on the sample manipulator. The excessive contribution due to scattered γ-rays is evident not only in the intensity of the backscatter peak (at ≈1/3 m_0c^2) but also in the uncommon flatness of the Compton continuum below the edge (at ≈2/3 m_0c^2).

To investigate this further a "benchtop" simulation was arranged.[9] Using a similar detector and a ^{85}Sr source a series of scatterers and absorbers were assembled to simulate the physical environment of the beam, as judged by the shape of the total measured annihilation energy distribution. The final arrangement is shown in Fig. 3 together with the measured distribution [curve (a), solid line], indicating good qualitative agreement with the distribution in Fig. 2. In order to see how much of the simulated spectrum is made up of scattered radiation, we subtracted from it the spectrum obtained by putting another (much weaker) ^{85}Sr source directly on the detector face and running without scatterers until the full-energy peak went to zero. This difference is shown in Fig. 3(b) (dashed line). It is clear from these two curves that more than half of the counts at energy lower than the photopeak must be attributed to scattering. It is particularly noteworthy that there is a region in the valley where close to 75% of the counts are due to scatter. This is just where one would hope to have a predominance of events due to the 3-γ decays of ortho-Ps in order to optimize sensitivity to changes in f.

The previous discussion of γ-ray scattering highlights the primary objection to acquiring data with the detector mounted at the side, as

illustrated in Fig. 1. Since most of the 511 keV radiation originates at or near the surface of the specimen, small variations in the specimen angle (with respect to the detector face) can lead to significant changes in the "shadowing" of the detector. The samples studied typically have areal dimensions of about 1 inch^2, whereas the incident beam is only a few mm in diameter. This means that those γ-rays which pass through the specimen towards the detector must pass through on the order of 1 cm of metal absorber/scatterer. The effect of small rotations of the sample about the manipulator axis is demonstrated in Fig. 4, where variations of 10% in f are found with rotations of less than 10 degrees. $\theta = 0°$ is defined as the position where the sample face is perpendicular to the detector face, and positive rotation is towards the detector.

The last effect we will discuss in this section is the variation of R with total countrate. This has obvious application since positron beams are often based on ^{58}Co sources[8] ($T_{1/2}$ = 71 dy), and determinations of the "reference" values R_0 and R_1 are not necessarily performed at the same time as a particular experiment. Once again a Ge(Li) detector was used with an Ortec 572 amplifier (3 μsec time constant). A ^{64}Cu source was allowed to decay ($T_{1/2}$ = 12.8 hr) while spectra were continually acquired both with and without pileup rejection. The peak integral was taken from ≈500 keV to ≈520 keV. The results shown in Fig. 5 indicate only a small effect of countrate from ≈0 up to 24 K cps, particularly while using pileup rejection (≈1% decrease in R for 15 K cps total change in rate.)

III. Incident Positron Backscattering

The backscattering of positrons emitted from an isotopic source (such as ^{22}Na) has been studied by several researchers.[10-12] MacKenzie et al.[11] found that the backscatter coefficient, R, was adequately described by a logarithmic function of the atomic number, Z, of the scattering material. Their measured coefficients using both ^{68}Ge and ^{22}Na were in general consistent with calculations[31] for monoenergetic positrons in the 0.1-1.0 meV energy range over a broad range of Z. These same calculations predicted a similar (although slightly larger for all Z) coefficient for electrons than for positrons.

Relatively little has been done for low energy positrons, with the exception of the measurements of Mills and Wilson[14] who studied monoenergetic positrons ranging from 0.5 to 2.9 keV scattering off an Al specimen. They found that the total scattering probability (r) was <10% in all cases, increasing from r ≈4% at 500 eV to r = 10% at 2.9 keV. These data would seem to be in disagreement with the result of Darlington and Cosslett,[15] who found that r decreases for electrons as a function of increasing electron energy, ranging from r = 44% at 500 eV to r = 28% at 3.0 keV. In view of the aforementioned predictable similarity of the results for positrons and electrons at high energy, it would seem that this discrepancy in both sign and magnitude of the r vs. E behavior is important. It is possible that the difference arises from the effect of low-energy positrons being channeled[16] into the interstitial regions of the lattice and electrons being preferentially attracted towards the ion cores, however there are presently too few measurements upon which any quantitative comparison can be based. It is clear that the problem of incident positron beam scattering needs more attention, since the

energy dependence would have obvious implications to the understanding of experimental results.

IV. Relationship of $(P_1)/(P_0)$ to f

As mentioned in the introduction, the reference states of 100% and 0% Ps are often difficult to achieve. This affects f not only through the respective ratios R_1 and R_0 (discussed in section V), but also through the peak integrals necessary for the prefactor P_1/P_0 in eq. (13). Because this ratio determines exactly how f is related to R, errors in P_1/P_0 can lead to serious non-linearities, unlike errors in either R_1 or R_0 alone (sec. V). This is demonstrated in Fig. 6, where f is plotted versus R for two values of P_1/P_0; the abscissa is scaled to be zero at $R = R_0$ unity at $R = R_1$.

The value of P_1/P_0 is traditionally obtained empirically, just as the individual ratios R_1 and R_0 are. The measurement of the 100% Ps state is (at Brookhaven) based on the saturation value of f observed[17] when Al with a submonolayer oxide coating is heated to high temperatures, and implanted with very low energy ($E < 25$ eV) incident positrons. A similar saturation value (leading to the conclusion that 100% Ps is formed) has been observed for Cs on Si.[18] In both cases the assumption that the surface trap normally observed[3,4] is removed by the overlayer is justified by heating above the desorption temperature. The 0% Ps state is not quite so difficult to attain. It requires only that positrons are implanted in the specimen with sufficient energy such that few, if any, will diffuse back to the surface where Ps is formed. Up until now the primary limitation has been positron beams that provide

maximum energies of between 5 and 20 keV, and so defected crystals (produced by sputter-ing bombardment) which trap positrons are sometimes used to ensure that positrons will not escape.

In general what we find is that $P_1/P_0 = 0.42 \pm 0.05$ when using a Ge(Li) or intrinsic Ge detector, and it seems to be fairly independent of variations in environment such as scattering, countrate changes, etc. This independence does not, of course, apply to either R_1 or R_0. It is possible to estimate with reasonable accuracy what the value of P_1/P_0 should in fact be, since most of the effects which are difficult to estimate cancel out of the expression. In the discussion that follows we shall attempt to estimate P_1/P_0, a summary of the results being listed in Table 1.

We begin with the basic assumption that ortho-Ps is 3 times as plentiful as para-Ps. Although this has never been proven, it is based on relatively straightforward kinematic arguments[5] and is certainly close to the truth. Ortho-Ps decays with 3 γ-rays that produce a roughly triangular energy distribution[5] that increases from zero at 0 keV to a maximum at 511 keV. We will take the peak integral with 0% Ps to be 1.0, and therefore that with 100% Ps (25% of which is para-Ps) is 0.25. The expression for P_1/P_0 can be written:

$$\frac{P_1}{P_0} = \frac{0.25 + \sum_i P_1(i)}{1.0 + \sum_i P_0(i)} \qquad (14)$$

where the terms $P_1(i)$ and $P_0(i)$ are additive corrections to the probability that counts will fall in the peak integral for 100% and 0% Ps, respectively.

The first and most obvious correction arises due to the fact that a small fraction of the ortho-Ps decays will be included in P_1. Assuming the peak "window" is ±12 keV (allowing ±3 keV variation), then this correction (for a triangle) is ≈0.046±0.011 (total enclosed area) × 75% (ortho-Ps decays) ≈ 0.035±0.008. Since ortho-Ps decays by 3 γ-rays, then there is a 3/2 probability of detection relative to either para-Ps or unbound positron annihilation (2 γ-rays). For a rear-mounted detector (Fig. 1) this enhancement is largely cancelled by other factors:

(1) Ps has, in general, kinetic energy that arises from the Ps work function--which varies from ≈1 eV to ≈5 eV.[1,2] Assuming a value of 2.7 eV,[19,20] about half of the ortho-Ps travels ≈10 cm from the sample face (away from the detector). To a good approximation, the resulting reduction in detection efficiency almost entirely cancels the enhancement introduced by the 3:2 γ-ray ratio.

(2) Re-emitted ortho-Ps is something like 10 to 15% polarized along an axis perpendicular to the crystal face.[20] Of this fraction, approximately 1/3 (m = 0) decays with γ-rays being emitted preferentially perpendicular to the axis of polarization,[21] hence having virtually no probability of being detected by a rear-mounted detector. The total effect is small, reducing the detection probability for ortho-Ps by ≈0.10×0.33, or about 3%.

The net result is that the P_1 correction for ortho-Ps,is unchanged from the 0.035 calculated above. This value is not critical, but it is more empirical than analytical, based on the observation that our total countrate changes very little as a function of Ps.

The second correction which must be applied is due to 511 keV background from annihilations of the incident positrons in the accelerator

grids (see Fig. 1). Since we normally use a pair of 90% transmission Mo grids, we will base the correction factor calculation on 81% transmission. Using a probability of 1.0 for peak counts at the sample with 0% Ps, and allowing for a 25±3% geometrical efficiency for annihilations arising in the grids relative to those at the sample, the total correction (to be applied to both P_1 and P_0) is given by

$$\left(\frac{1.0}{0.81}\right) \times 0.19 \times 0.25\ (\pm 0.03) = 0.059 \pm 0.007$$

where (1.0/0.81) is the relative incident beam intensity before passing through the grids.

There are several other factors which influence P_1/P_0, but which are insignificant relative to those already discussed. We include in these room background counts, moving Ps effects (e.g. red shift and/or pickoff), γ-ray absorption and scattering effects (more important at $E \ll 511$ keV), and summation of 2 ortho-Ps γ-rays (from one decay) due to finite detector size. The result (Table 1) of the corrections considered is that the calculated ratio (0.32) is about 20% less than the measured ratio (0.42)

One way to account for this discrepancy would be to assume the basic 3:1 ratio of ortho to para-Ps is wrong. This seems unlikely since it would have to be less than 2:1 to fully account for the difference. Alternately, if 10% of the ortho-Ps decayed by 2 γ-ray emission this would also account for the difference. This could arise from spin exchange or pickoff almost immediately following the Ps formation at the surface, before it has moved too far to be influenced by "spill-out" electrons. Although the details of Ps formation at the surface of a metal are still uncertain, this last possibility seems unlikely in light

of the time scale involved; Ps with 2 eV kinetic energy travels ≈6000 Å in 1 psec.

Another possibility which would explain the discrepancy is that some fraction of positrons that are deposited at a surface have zero probability of forming Ps under any of the experimental conditions studied so far. Once again, this fraction would have to be ≈10% to fully explain the difference. On the basis of all the data obtained so far with positron beams it is impossible to determine whether or not this explanation is valid. The only direct measurement of Ps fraction that has been done employing triple coincidence[22] does not preclude this possibility.

Perhaps the most likely source of the discrepancy is scattering of the incident positron beam, as discussed in section III. In order to measure P_1/P_0 one typically assumes a constant beam flux, acquiring data for a fixed time. What is really needed is not constant time but constant number of positrons. If, in fact, more incident positrons are scattered out of the region of detection during the measurement of P_0 than for P_1, the measured P_1/P_0 ratios would be increased. Since P_0 is typically measured at high incident energy (<5 keV) and P_1 at very low energy (≈25 keV) this possibility is supported by the observation[14] that the backscattering probability increases with energy in this range. On the other hand, the magnitude of the scattering coefficient required at 5 keV to completely explain the discrepancy is ≈24%, which is somewhat larger than would be expected on the basis of the coefficients measured previously.[14]

V. Statistical Error for f

In using the dependence of f on positron energy to deduce model parameters by least-squares fitting (section VII), it is essential to weight the data with errors propagated from the raw counts. For the errors in R (Eq. 11), a binomial distribution is used, similar to the approach used to obtain errors for s-parameters from Doppler-broadened positron sp... ...a.[23] The result

$$\sigma_R^2 = \frac{R(R+1)}{P} \tag{15}$$

gives smaller error estimates than a straightforward Poisson statistics analysis using the square root of the counts as errors ($\sigma_P^2 = P$, $\sigma_T^2 = T$) viz.

$$\sigma_R^2 = \frac{(R+1)(R+2)}{P} \tag{16}$$

The dependence of f on R (Eq. 13) is shown in figure 6 for two values of P_1/P_0. The standard uncorrelated error in f is given by

$$\sigma_f^2 = f^2(1-f)^2\left\{\frac{\sigma_{P_1}^2}{P_1^2} + \frac{\sigma_{P_0}^2}{P_0^2} + \frac{\sigma_{R_1}^2}{(R_1-R)^2} + \frac{\sigma_{R_0}^2}{(R-R_0)^2} + \sigma_R^2\left[\frac{1}{R_1-R_0} + \frac{1}{R-R_0}\right]^2\right\} \tag{17}$$

The error propagation factors for the values that enter this formula are shown in figure 7 for $P_1/P_0 = 0.5$. It should be noted that relative errors are reduced during propagation, especially for P_1/P_0 where eg. a 10% error gives a 2.5% (maximum) error in f.

VI. Simulation: Propagation of Endpoint Errors

The method employed was to generate theoretically expected γ-ray energy distributions for known fractions of Ps, and to convolute these

data with measured response functions for 3 different detection systems which are representative of those normally used in slow-positron studies.[3,4] Para-Ps was assumed to be a δ-function centered at 511 keV, and ortho-Ps was generated viz:[5]

$$O(k) = 2\left[\frac{k(m-k)}{(2m-k)^2} - \frac{2m(m-k)^2}{(2m-k)^3}\ln\left(\frac{m-k}{m}\right) + \frac{2m-k}{k} + \frac{2m(m-k)}{k^2}\ln\left(\frac{m-k}{m}\right)\right] \quad (18)$$

where $k = E_\gamma/mc^2$. The intensity of the ortho-component was set at 3 times that for para-Ps. Free positron annihilations were assumed to occur with the electrons of a fairly typical metallic sample, and the energy spectrum was therefore represented by an inverted parabola atop a Gaussian. The parabola intensity was set at 3/2 that for the Gaussian, and the width at the base of the parabola was 0.6 times the FWHM of the Gaussian. Because this width represents the momentum broadened Fermi energy (which was chosen to be 12 eV), this established the Gaussian FWHM = 4.1 keV.

The detectors used were: (a) a PGT Ge(Li) detector with a resolution of about 1.5 keV FWHM at 514 keV; (b) a 3"×3" Harshaw NaI(Tl) detector with a resolution of about 40 keV FWHM at 514 keV; (c) a 3"×3" NaI(Tl) crystal on a 48" right-angle light pipe, with a resolution of about 120 keV FWHM at 514 keV. Detector (c) was designed so that the photomultiplier would not be affected by the magnetic field required by the positron beam transport,[8] while the crystal "viewed" the specimen from behind (on the magnetic field axis). A comparison of two theoretical spectra generated for detector (c) with real data obtained previously with the same detector are shown in Fig. 8.

The sources used to determine the response functions for all the detectors were ^{57}Co (122 keV with some 136 keV), ^{198}Au (412 keV) and ^{85}Sr (514 keV). The theoretical energy distribution was convoluted with the response function measured for each of these sources; the ^{58}Co spectrum was applied to the range 0 to ≈200 keV, the ^{198}Au was applied from ≈200 to 450 keV, and the ^{85}Sr was applied from ≈450 to 511 keV. The variable peak-to-Compton ratios and scattering properties associated with γ-rays of different energies would be best represented by measuring a large number of clean, single γ-ray standards (were such a selection available). We feel, however, that our spectra were suitably produced for the purpose of this study using these three sources, since the bulk of the information (hence systematics) arising from the positron plus Ps annihilation spectrum is in the vicinity of 511 keV. The favorable comparison seen in Fig. 8 supports this statement. Spectra were normalized to 2×10^6 counts, and each data point was randomized according to a normal distribution for which $\sigma = n_i^{1/2}$, where $n_i \equiv$ counts in the ith channel.

In figure 9 we show the results of using the simulated spectra to calculate f, the Ps fraction, according to eq. (13). The differences between the calculated and known f's are plotted versus the known f's for both f_p [Fig. 9(a); peak area] and f_v [Fig. 9(b); valley area]. It is evident from this figure that although the valley gives a profound visual response to changes in the Ps fraction, it is as much as a factor of 10 less precise than an f derived from the peak. In addition, the γ-ray scattering already discussed in section II (fig. 3) would cast some doubt on an analysis using the valley counts. The plot of f_p also illustrates that both of the "better" detectors yield reasonable

results, giving reliable measurements to better than half a percent. This is consistent with the conclusions reached in section II. In addition, we found that the precision of the "worst" detection system is somewhat dependent on the selection of the summation region, and have shown in Fig. 9(c) the results of selecting a narrower region for the peak. It is clear from this that the best detection system must have moderately good resolution in order to minimize systematic errors in the determination of F, including those not included in this simulation such as instrumental drifts and countrate effects.

The discussion so far has been based on the assumption that both the extreme conditions of 0% and 100% Ps are measurable (or can at least be accurately extrapolated). As a test of the significance of this, we altered the calculations of f by introducing errors of ±5 to ±10% to the endpoint ratios, R_0 and R_1. We found this to have no non-linear effect on the data unlike errors in P_1/P_0 discussed in section III. The only effect was to shift curves essentially like those in figure 9 up or down at either end by the amount equal to the error that was introduced. Aside from this, the relationship between the measured f and the "true" f remained linear.

VII. Calculation of Positron Diffusion Lengths

The absence of any non-linear contributions to the deduced Ps-fraction for real data lends confidence to the method commonly applied[24] to measurements of the positron diffusion length, L_+. The application of a one-dimensional diffusion model relates f to incident positron energy, E:[3,17]

$$f = \frac{f_0}{1 + (E/E_0)^n} \qquad (19)$$

where n is usually about 1.6.[17,25] There is, in fact, a fair degree of uncertainty in the derived value of n for various materials. Although n is very nearly 1.6 for "light" materials such as Al[17] and Si[26], it appears to have some dependence on atomic number. For example, n = 1.4 for Ge[27] and Cu[28]. In addition, n is often observed to be reduced by the introduction of crystal imperfections, being ≈1.34 for n-irradiated Al[29] and as low as ≈1.0 for thermally generated vacancies in Al[6]. It is clear that obtaining the best value for n is of particular importance, as is demonstrated in Fig. 10. The relationship of f and incident positron energy E can be seen to depend critically on the value of n, although the detailed shape of the curve itself is often the best indication of the true value. The expression shown in Fig. 10 [eq. (19)] results from an exponential positron implantation profile, however the profound dependence of the curve on the factor n has analogous complications using other profiles.[30] E_0 can be related to the positron diffusion coefficient D_+ by the expression:

$$E_0^n = \frac{\sqrt{D_+ \tau_{eff}}}{A} \qquad (20)$$

where τ_{eff} is the effective lifetime of the positron in the sample,[29] and $L_+ = (D_+ \tau_{eff})^{1/2}$. A is a constant that relates E_0 to mean depth, α, through the function:

$$\alpha = AE_0^n \qquad (21)$$

Mills and Wilson[25] have found that $A = (3.32^{+0.84}_{-0.70})$ μg/cm^2, with E_0 in keV.

Recently there has been interest in establishing E_0 through the energy dependence of a standard annihilation lineshape parameter,[31] such as S,[32] which measures the relative fraction of events that fall in a fixed central portion of the peak. An identical diffusion model in eq. (19) has been applied,[31] based on the assumption that changes in the relative fraction of incident positrons that are re-emitted as Ps change the lineshape parameter linearly.

Figure 11 shows the result of calculating the S-parameter for the simulated spectra generated with the response function of the Ge(Li) spectrometer system (section VI). It is clear from this result that variations in the Ps fraction contribute more complicated changes to the annihilation lineshape than can reliably be accounted for by the simple model reflected by eq. (19). The extent of the error introduced can be assessed by choosing a set of data (f vs. E) that lead to a typical E_0 value for a common metal. Table 2 lists data chosen specifically to yield E_0 = 5.0 keV when fit to eq. (19), and the subsequent f's that would be deduced from the S-parameters shown in Fig. 12. The systematic error of this method of analysis leads in this case to a value of E_0 = __ keV (n = 1.6). Alternatively a non-linear fit to eq. (19) yielded E_0 = __ keV, with n = ____, and a slightly better fit.

VIII. Red-shift Due to Ps Energy

The last feature to be investigated with the simulated spectra was the effect of the Ps kinetic energy in red-shifting the peak. There is also a false red-shift observed due to the increase in o-Ps, which was demonstrated previously by Leventhal.[33] Figure 12 shows the peak-position (mode) for the simulated distributions discussed in section

VI. The false red-shift due to the ortho-Ps is seen in this figure to be exaggerated in the detectors with poor resolution. This effect would lead to an even larger shift of the centroid of the peak. The data shown in Fig. 12 were generated assuming the Ps had no kinetic energy as it left the surface of the crystal.

In addition to this we generated a set of spectra for which the Ge(Li) detector was assumed to be behind the crystal, and the Ps was emitted from the surface with 1.0 eV kinetic energy. Mills and Pfeiffer[19] have demonstrated that Ps emitted from a Cu(111) surface can have mean kinetic energies that range from ≈0.14(1) eV (for thermally activated) to 3.4(3) eV (non-thermally emitted).

For the present study it was assumed that the Ps is ejected with an isotropic distribution about the normal. If the spatial distribution is peaked about the normal, it would tend to increase the magnitude of the red-shift we have calculated. The data at each point in the energy distributions (arising from Ps annihilations) were red-shifted with a linear Doppler shift to account for this effect:

$$E' = E\left(1 - \frac{v \cos\theta}{c}\right) \tag{22}$$

where the velocity is:

$$v = \left(\frac{2E_k}{(2m_0)}\right)^{1/2} = 4.2\times10^7 \text{ cm/sec} \tag{23}$$

for $E_k = 1.0$ eV. The next effect which needed consideration was that the long-lived ortho-Ps (τ = 140 nsec) would travel significantly further from the detector than either "bulk" positrons or the short-lived para-Ps (τ = 125 psec). An estimate of the maximum distances travelled can be obtained by using the time 2τ, which means that $1/e^2$ or ≈1/10 of

the Ps atoms will travel that far. For ortho-Ps with E_k = 1.0 eV, d(2τ) = 11.7 cm, while for para-Ps d(2τ) = 0.009 cm. Because the geometrical reduction in detection efficiency would be significant for ortho-Ps we reduced all counts in the theoretical distributions arising from ortho-Ps annihilations by a factor which we now describe. By taking data from a chart of absolute detection efficiency ε versus distance d for a 2" × 2" NaI(Tl) crystal,[34] we were able to develop a polynomial expansion for ε(1/d) which we applied to our data. It was felt that the application of this to a Ge(Li) detector would be a reasonable approximation, since we were only interested in relative efficiency corrections. The derived expansion was:

$$\varepsilon = 1.0 - 19.25(1/d) + 5.9(1/d^2) - 0.67(1/d^3). \qquad (24)$$

The net result of the above corrections for Ps kinetic energy was to further (red) shift the centroid of each peak by an amount that was proportional to the Ps fraction. This is illustrated in figure 13. The effect is significant, indicating that this may be an alternative[19] way to measure the Ps kinetic energy.

IX. Other Methods for Determining f

Of the various techniques for measuring Ps one of the most direct is 3-γ coincidence,[6] since it provides an absolute determination of the relative fraction of events which arise from the decay of ortho-Ps. This has recently been used, for example, in measurements of the hyperfine interval between singlet and triplet Ps,[35,36] where a large number of detectors are arranged in a ring around the chamber to improve the triple coincidence probability. In general, the countrate and geometry limitations of this method are too restrictive for application

to positron beam studies of Ps, which are primarily applied to positron diffusion-length measurements (Section VII).

Two-γ coincidence as measured with a pair of NaI detectors has been applied to gas-quenching studies of Ps,[37] where the ortho-Ps fraction is deduced from the attendant decrease measured in the rate of 511 keV γ pairs. This technique is particularly useful in high-background situations owing to the intrinsic collimation afforded by the coincidence requirement. Although background is not usually a problem in positron beam experiments, it is interesting to speculate that useful information may be derived through the sum/difference technique which employs a pair of high-resolution solid state detectors.[38] The extremely low background and resolution improvement relative to the single detector measurements discussed in this report may for some applications justify the loss of countrate.

High resolution angular correlation (ACAR) measurements are another way in which Ps has been studied in various non-metallic solids.[39] Although this technique is not presently employed with positron beams, there is some hope that reactor-based beams will provide sufficient intensities to allow useful angular correlation studies not only of Ps, but also of the positron surface state.[40] Recent advances in 2-dimensional angular correlation[1] suggest that interesting studies of Ps may be pursued through the combination of 2-D ACAR and variable-energy beams. That this has not yet been done is simply a reflection of the difficulty and expense associated with the two techniques.

The only other technique for studying Ps that has had significant application to beam studies is lifetime measurements. This has the advantage of being a relatively direct and quantitative measurement,

like the 3-γ coincidence method, without being as severely limited by countrate. The primary difficulty lies in deriving a "start" signal, since the specimen is isolated from the actual positron source. This has so far been accomplished by synchronized time-bunching of a magnetically confined beam[41] and by detection of secondary electron emission (generated by the impinging positron) for an electrostatically focussed beam.[42] In one case the Lyman α emission from the $2^3S_1 \rightarrow 2^3P_2$ transition was used as the start signal for a measurement of a fine structure interval in an excited state of Ps.[43] It seems likely that both lifetime studies and the single detector technique discussed in this report will remain the dominant techniques for studies of Ps using variable-energy positron beams.

X. Summary and Recommendations

In this paper we have studied several aspects of the method of analyzing Ps fraction (f) data obtained with slow positron beams. We have shown that several systematic and experimental features are worthy of concern:

(a) γ-ray scattering in the vacuum chamber and associated equipment constitutes more than half of the counts below the full-energy peak, where the sensitivity to Ps is maximum.

(b) The dependence of backscattering (of the incident beam) on positron energy is currently unresolved.

(c) Uncertainties associated with the reference states of 100% and 0% Ps formation are particularly important. Although errors in peak:total (R) ratios individually do not appear overly important, the P_1/P_0 ratio (discussed in section IV) introduces clearly non-linear effects to the calculation of f.

(d) Calculation of the positron diffusion length, L_+, from f is influenced not only by the accuracy of f but also by the details of the positron stopping profile. In addition, the evidence indicates that calculation of L_+ based on annihilation lineshape parameters may suffer from a non-linear relationship of the parameters with f.

On the basis of the information presented in this paper the following recommendations can be made:

(i) Calibration of the 100% Ps state is essential if Ps fraction experiments are going to continue to be used in the areas of positron diffusion and surface interactions. This may be accomplished through more precise determinations of the triple-coincidence rate.[22]

(ii) The 0% Ps state also requires more careful determination than has been possible in the past. This problem has become more important in light of recent controversy over positron implantation profiles.[44] Positron beams capable of 50 keV (or more) incident energy may alleviate this problem if the present uncertainty in incident positron backscattering is resolved.

(iii) In the special case of materials which possess a negative positron work function, there may be some advantage in correlating diffusion lengths calculated using both f and direct re-emitted positron counting. Although the later techique is generally much more time intensive than Ps fraction measurements, it has the obvious advantage of being easily calibrated.

(iv) Problems associated with absorption and scattering of γ-rays should be minimized. This involves rear-placement of the detector (rather than side-placement) and ensuring that the amount of scattering

material between the sample surface and detector remains relatively constant.

(v) Calculation of f is best performed using a total:peak rather than total:valley type of ratio. In addition, the detector resolution should be as good as possible (without sacrificing too much efficiency) to ensure that the peak integral completely encompasses the photopeak without significantly overlapping the region of the spectrum where 3.8 events dominate. The present standard is to use large (≈20%) Ge(Li) or intrinsic Ge detectors.

We are indebted to I. K. MacKenzie for pointing out the significance of γ-ray scattering and performing the measurement shown in Fig. 3. We would also like to thank D. W. Gidley for his comments and suggestions. This work is supported by the Division of Materials Sciences, U.S. Department of Energy, under contract DE-AC02-76CH00016.

References

1. Positron Annihilation, Proc. of 6th Intl. Conf., P. G. Coleman, S. C. Sharma and L. M. Diana, eds., North-Holland Publ. Co. (1982).
2. See papers by A. P. Mills, Jr. and K. G. Lynn in International School of Physics, "Enrico Fermi," edited by W. Brandt and A. Dupasquier (1981) (in press).
3. A. P. Mills, Jr., Phys. Rev. Lett. 41, 1828 (1978).
4. K. G. Lynn, J. Phys. C 12, L435 (1979).
5. A. Ore and J. L. Powell, Phys. Rev. 75, 1696 (1949).
6. M. Deutsch, Progr. Nucl. Phys. 3, 131 (1953).
7. V. W. Hughes, S. Marder and C. S. Wu, Phys. Rev. 98, 1840 (1955).
8. K. G. Lynn and H. Lutz, Rev. Sci. Instrum. 51, 977 (1980).
9. I. K. MacKenzie, previously unpublished data.
10. A. Bisi and L. Braicovich, Nucl. Phys. 58, 171 (1964).
11. I. K. MacKenzie, C. W. Schulte, T. Jackman and J. L. Campbell, Phys. Rev. A7, 135 (1978).
12. H. E. Hansen, S. Linderoth and K. Petersen, Appl. Phys. A29, 99 (1982).
13. V. A. Kuzminikh, I. A. Tsekhanovski and S. A. Vorobiev, Nucl. Inst. Meth. 118, 269 (1974).
14. Allen P. Mills, Jr. and Robert J. Wilson, Phys. Rev. A26, 490 (1982).
15. E. H. Darlington and V. E. Cosslett, J. Phys. D: Appl. Phys. 5, 1969 (1972).
16. J. A. Davies, private communication.
17 K. G. Lynn and H. Lutz, Phys. Rev. B 22, 4143 (1980).

18 Allen P. Mills, Jr., Solid State Commun. 31, 623 (1979).

19. A. P. Mills, Jr. and Loren Pfeiffer, Phys. Rev. Lett. 43, 1961 (1979).

20. A. P. Mills, Jr., private communication.

21. γ-ray correlation with ortho-Ps decay.

22. K. F. Canter, A. P. Mills, Jr. and S. Berko, Phys. Rev. Lett. 33, 7 (1974).

23. J. L. Campbell, Appl. Phys. 13, 365 (1977).

24. K. G. Lynn and D. O. Welch, Phys. Rev. B 22, 99 (1980).

25. Allen P. Mills, Jr. and Robert J. Wilson, Phys. Rev. A 26, 490 (1982).

26. K. G. Lynn, T. McMullen, and H. Jorch, to be published.

27. H. H. Jorch, K. G. Lynn, and I. K. MacKenzie, Phys. Rev. Lett. 47, 362 (1981).

28. P. J. Schultz and K. G. Lynn, unpublished data.

29. P. J. Schultz, K. G. Lynn, R. N. West, C. L. Snead, Jr., I. K. MacKenzie and R. W. Hendricks, Phys. Rev. B 25, 3637 (1982).

30. H. H. Jorch, K. G. Lynn, and D. O. Welch, to be published.

31. W. Triftshäuser and G. Kögel, Phys. Rev. Lett. 48, 1741 (1982).

32. I. K. MacKenzie, J. A. Eady and R. R. Gingerich, Phys. Lett. 33A, 279 (1970)

33. M. Leventhal, Astrophysical J. 183, L147 (1973).

34. Scintillation Phosphors Catalog, 3rd Edition.

34. A. P. Mills, Jr. and G. H. Bearman, Phys. Rev. Lett. 34, 246 (1975).

36. P. O. Egan, W. E. Frieze, V. W. Hughes and M. H. Yam, Phys. Lett. 54A, 412 (1975).

37. Richard Louis Klobuchar, Ph.D. thesis, Carnegie-Mellon University (1975).

38. K. G. Lynn, J. R. MacDonald, R. A. Boie, L. E. Feldman, J. D. Grabbe, M. F. Robbins, E. Bonderup, and J. Golovchenko, Phys. Rev. Lett. 38, 241 (1977).

39. A. Dupasquier in Positrons in Solids, Springer-Verlag (1979) pp. 197-244.

40. K. G. Lynn, private communication.

41. A. P. Mills, Jr., Appl. Phys. 22, 273 (1980).

42. D. W. Gidley, A. R. Köymen and T. Weston Capehart, Phys. Rev. Lett. 49, 1779 (1982).

43. K. F. Canter, A. P. Mills, Jr., and S. Berko, Phys. Rev. Lett. 34, 177 (1975).

44. S. Valkealahti and R. M. Nieminen, to be published.

Table 1

The factors involved with the calculation of P_1/P_0 discussed in the text [eq. (14)] are listed. Possible sources of the discrepancy shown at the bottom are discussed in the text.

	Peak Integral Contributions	
	$P_1(i)$	$P_0(i)$
Basic ortho:para ratio	0.25	1.00
(1) ortho-Ps counts in peak	0.035±0.008	0
(2) grid annihilations	0.059±0.007	0.059±0.007
P_1/P_0 (calculated)	0.32±0.01	
P_1/P_0 (measured)	0.42±0.05	
Discrepancy	0.10	0

Figure Captions

Figure 1. The ultra-high-vacuum (UHV) target chamber for the magnetically-guided positron beam at Brookhaven is shown, indicating the arrangement of components relevant to the discussion in the text.

Figure 2. A typical spectrum obtained for a rear-mounted Ge(Li) detector is shown, emphasizing the low energy portion of the distribution. The unusual shape--namely the flatness of the Compton continuum and the intensity of the backscatter peak--are indications of excessive γ-ray scattering in the vacuum chamber.

Figure 3. The contribution due to scattering is demonstrated by the simulation pictured above. The solid curve (a) is similar to the actual spectrum shown in Fig. 2 because of the proximity of metallic scatterers. The dashed curve (b) was obtained by removing the scatterers, placing a much weaker ^{85}Sr source directly on the detector face, and subtracting from curve (a) until the full energy peak just disappeared.

Figure 4. The effect of sample rotation on measurements of the Ps fraction, f, is shown for a side-mounted detector (see Fig. 1). The relative "flatness" for positive rotation (surface towards the detector) is due to the reduction of γ-ray absorption in the specimen, since most Ps annihilations occur just outside the front surface of the specimen.

Figure 5. The influence of total countrate on the R parameter used for calculation of f [eq. (13)] is shown both with and without

pileup rejection. The effect is small in both cases, however the improvement introduced through pileup rejection is obvious.

Figure 6. The non-linear dependence of the Ps fraction, f, on the total:peak ratio, R, [eqs. (11)-(13)] is shown for two different values of P_1/P_0 (peak counts with 100% and 0% Ps, respectively). The actual value of P_1/P_0 is approximately 0.4, although there has so far been no direct measurement of it.

Figure 7. The error propagation factor, ϵ, is shown for errors in the measured ratio, R, and the extremes used in equation (13) for $P_1/P_0 = 0.5$. The relative error in f can be seen to be less than that in R over the entire range.

Figure 8. The upper curves showing real spectra obtained for Al (estimate ~0% and 85% Ps re-emission) are to be compared with the lower simulated curves. Aside from certain deficiencies at the lowest energies, it can be seen that the comparison is reasonably good.

Figure 9. The error in calculating f with Eqn. 13 is shown for three different analyses. Data are shown for three different detection systems: for FWHM = 1.5 keV (at 514 keV), x for FWHM = 40 keV and Δ for FWHM = 120 keV. It is demonstrated that selecting a wide region for peak summation [curve (a) relative to curve (c)] leads to less uncertainty. The valley-type analysis [curve (b); summed over 410 to 430 keV] is seen to be less accurate than the peak-type.

Figure 10. The relationship of f to incident positron energy, E, is seen to be critically dependent on the exponent, n. The expression (inset) is for an exponential implantation profile, and the curves shown are for n = 0.5 up to n = 3.0, in steps of 0.5.

Figure 11. The annihilation lineshape parameter, S, is shown for the data generated for a typical Ge(Li) spectrometer as a function of the known positronium fraction, f. The nonlinearity evident from this curve leads to errors that are summarized in Table 2.

Figure 12. The false "red" shift in the peak position caused by differing amounts of positronium (Ps) is shown for the various spectrometers. For the purposes of this set of data, the Ps was assumed to have no kinetic energy. The detector resolutions are shown to the right of each curve.

Figure 13. The centroid shift introduced by 1.0 eV positronium kinetic energy is illustrated relative to 0 eV kinetic energy.

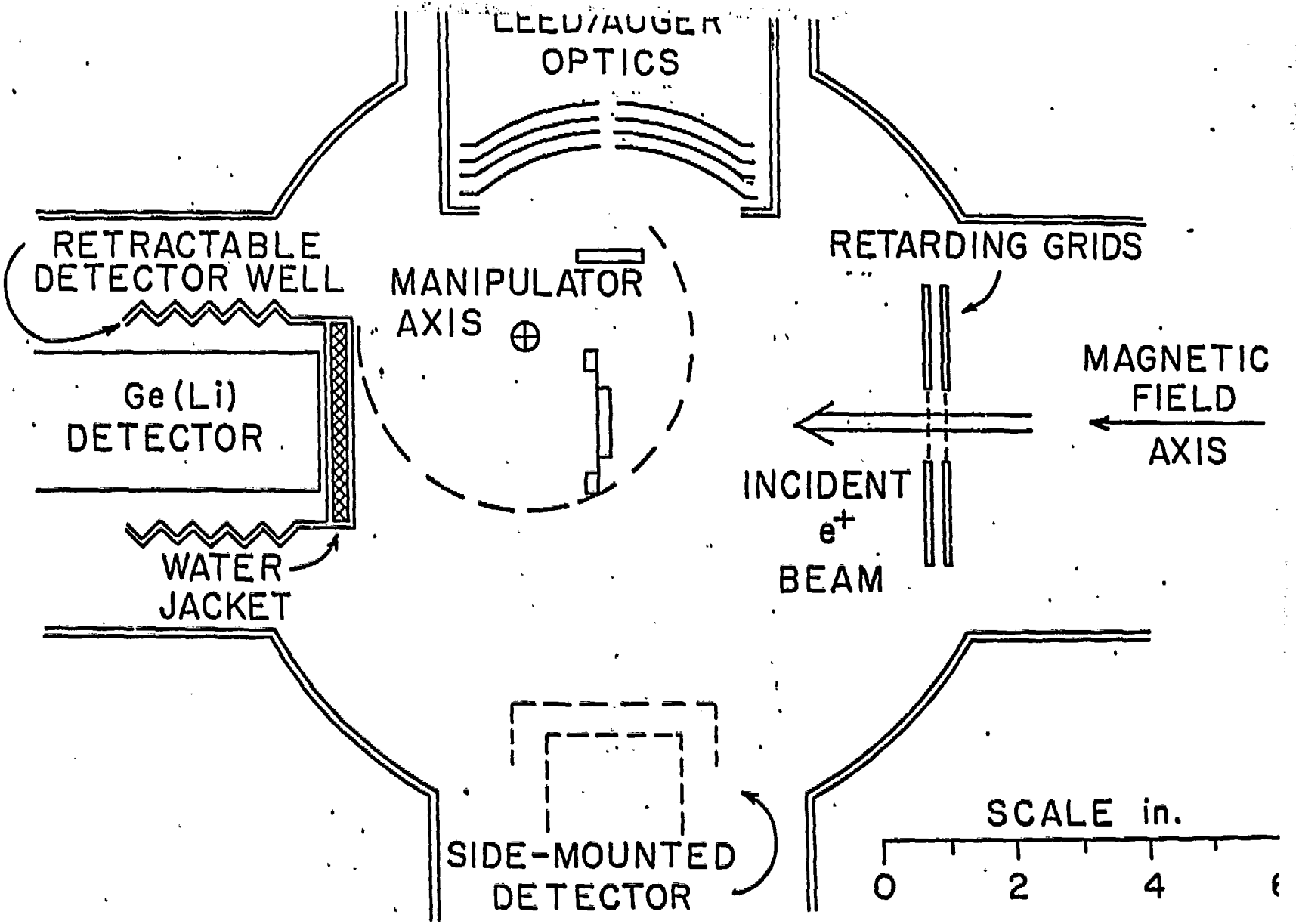
LEED/AUGER
OPTICS
RETRACTABLE
DETECTOR WELL
MANIPULATOR
AXIS
RETARDING GRIDS
Ge(Li)
DETECTOR
MAGNETIC
FIELD
AXIS
INCIDENT
e+
BEAM
WATER
JACKET
SIDE-MOUNTED
DETECTOR
SCALE in.
0
2
4

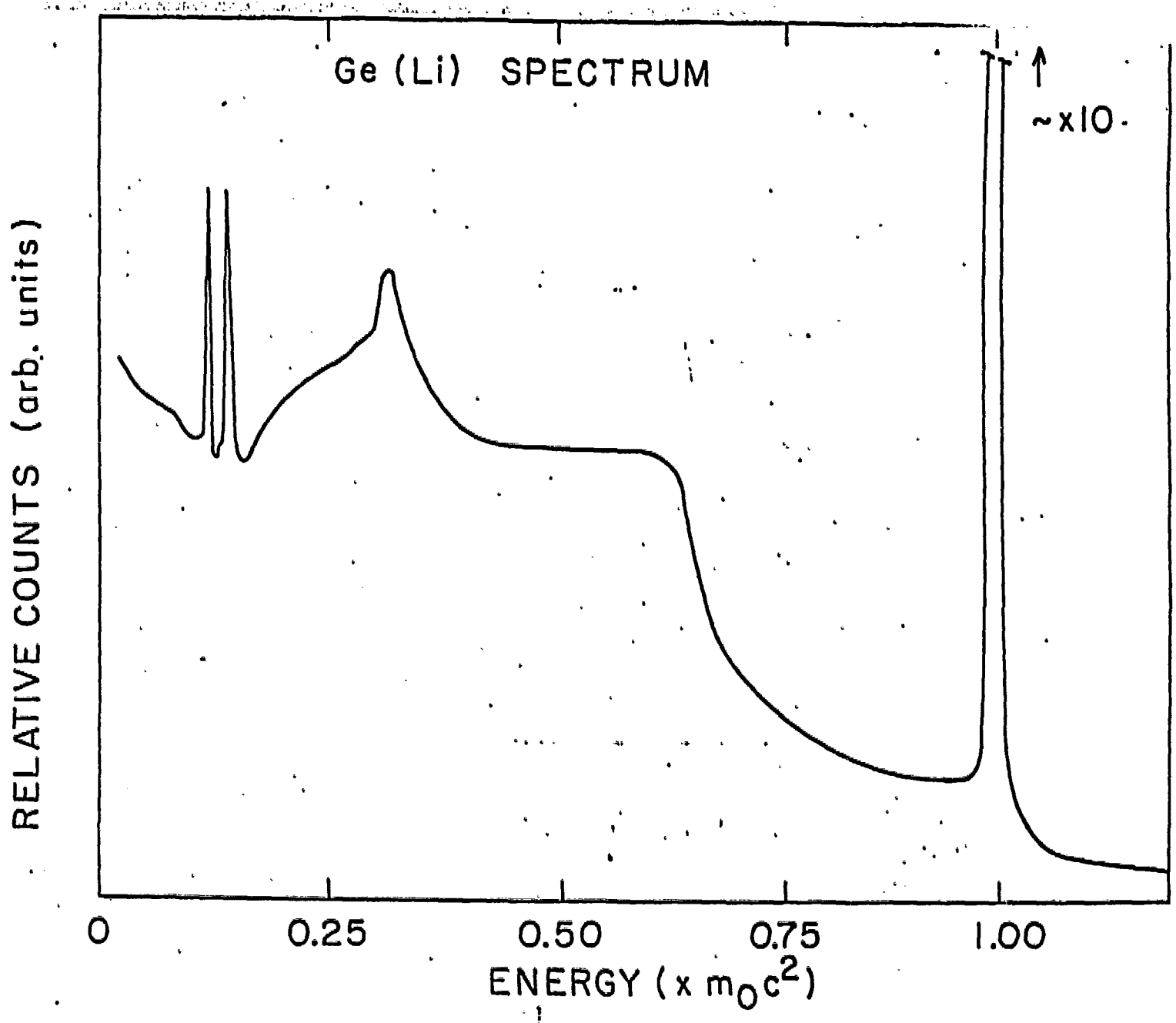
Ge (Li) SPECTRUM
~x10
RELATIVE COUNTS (arb. units)
0
0.25
0.50
0.75
1.00
ENERGY (x m_0c^2)

Fig 2

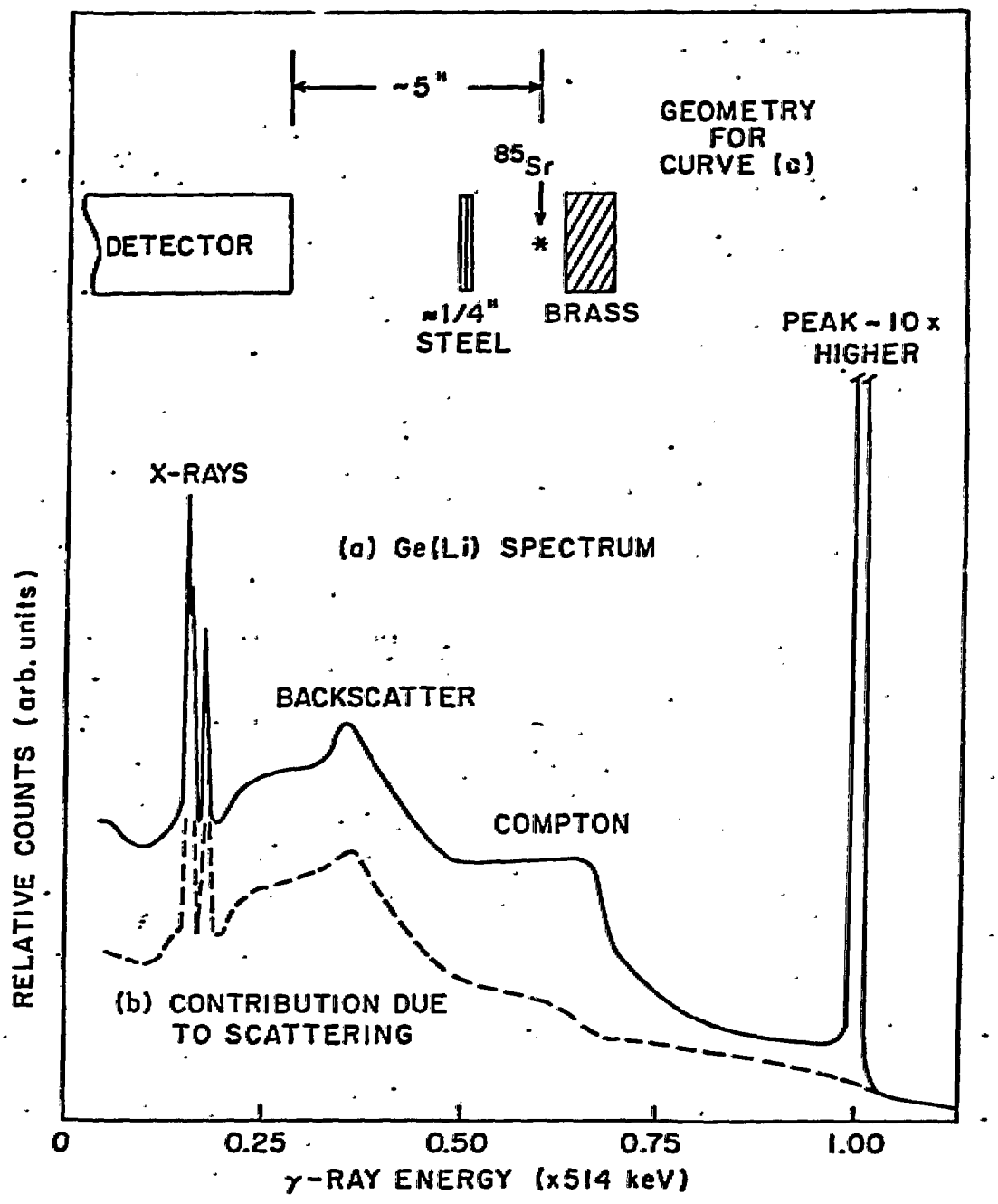
~5"
GEOMETRY FOR CURVE (c)
85Sr
DETECTOR
≈1/4" STEEL
BRASS
PEAK - 10 x HIGHER
X-RAYS
(a) Ge(Li) SPECTRUM
BACKSCATTER
COMPTON
(b) CONTRIBUTION DUE TO SCATTERING
RELATIVE COUNTS (arb. units)
0
0.25
0.50
0.75
1.00
γ-RAY ENERGY (x514 keV)

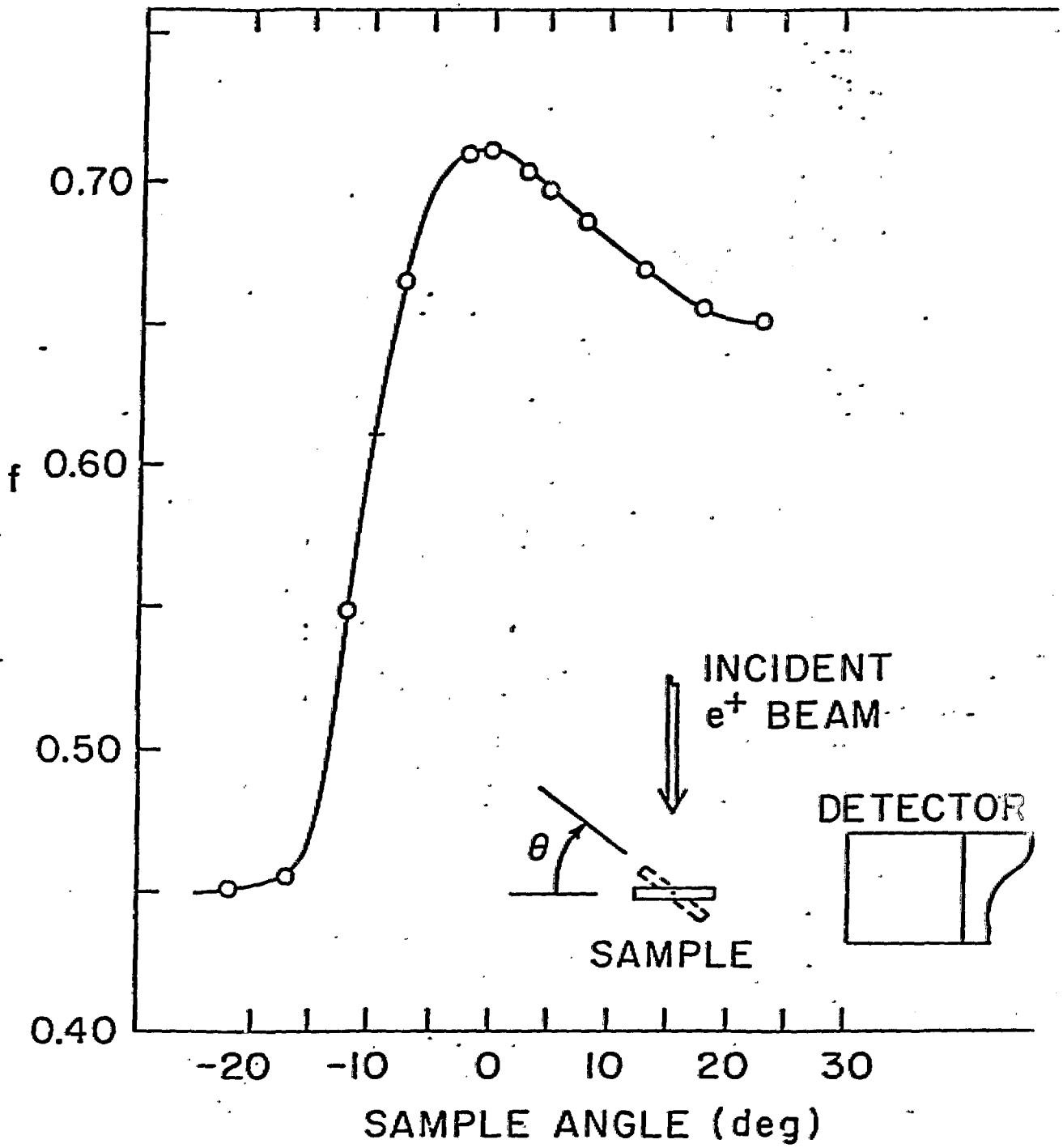
0.70
f 0.60
0.50
0.40
-20
-10
0
10
20
30
SAMPLE ANGLE (deg)
INCIDENT
e+ BEAM
θ
SAMPLE
DETECTOR

Fig 4

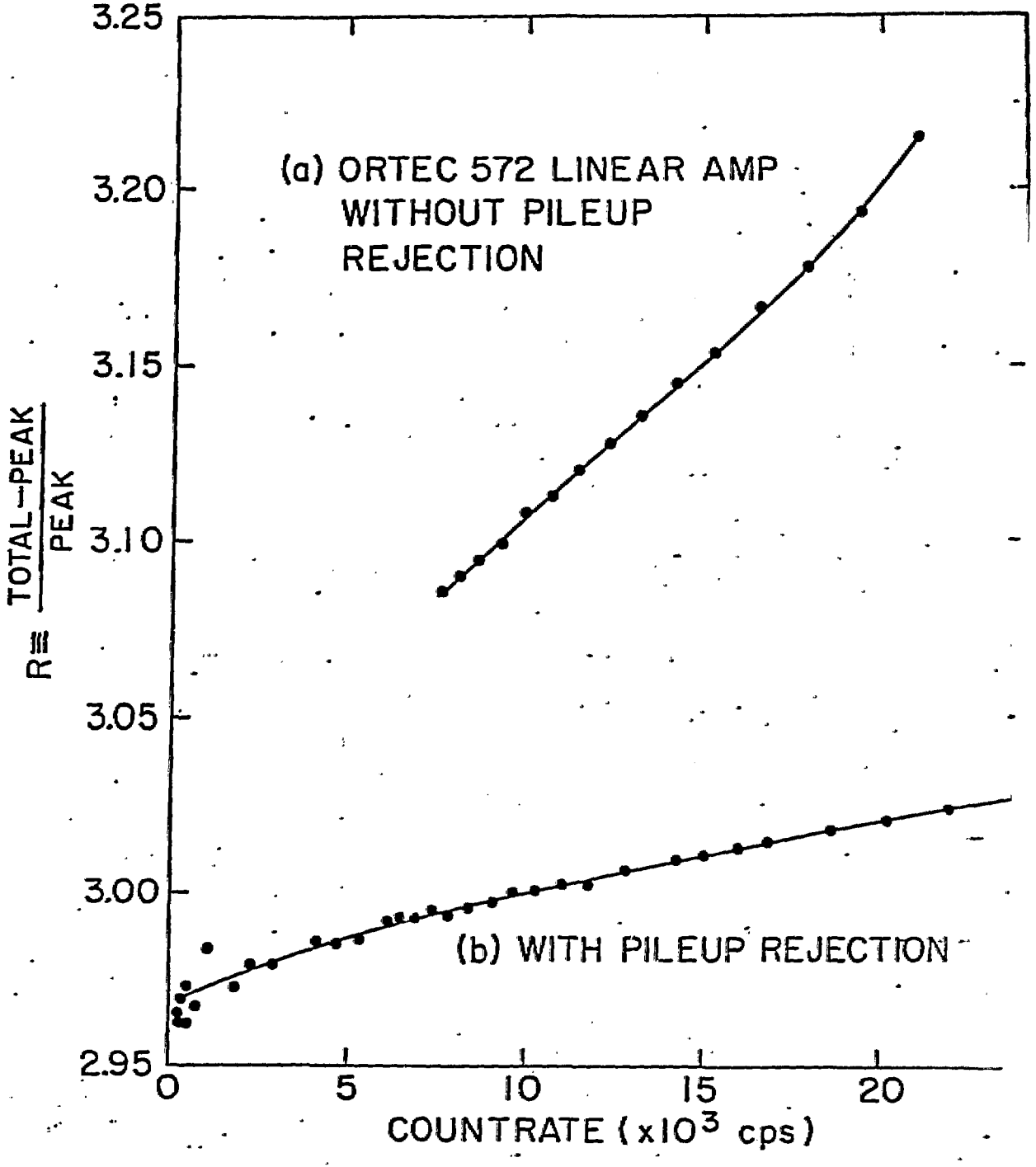
3.25
3.20
3.15
3.10
3.05
3.00
2.95
R ≡ TOTAL−PEAK / PEAK
(a) ORTEC 572 LINEAR AMP WITHOUT PILEUP REJECTION
(b) WITH PILEUP REJECTION
0
5
10
15
20
COUNTRATE (x10³ cps)

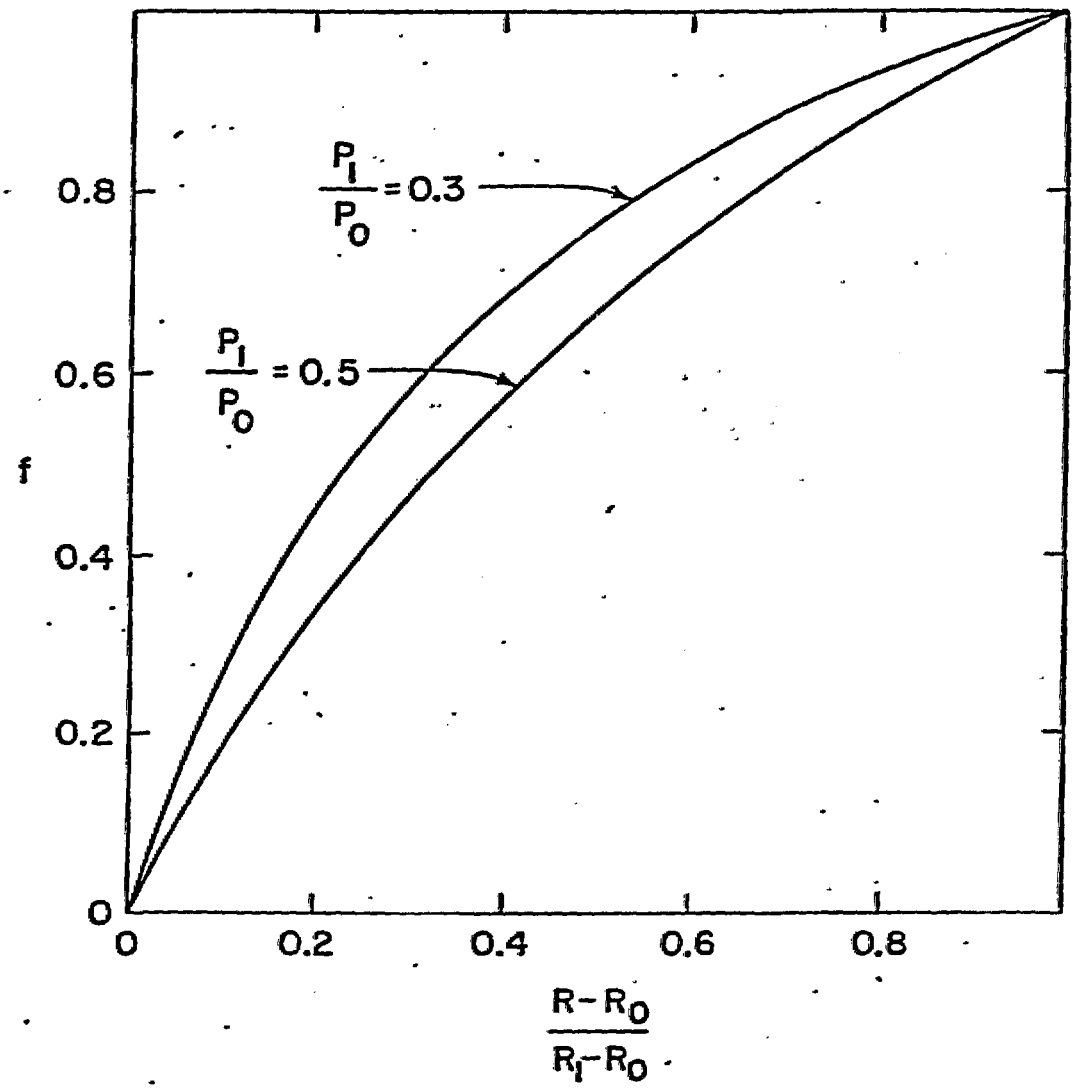
0.8
0.6
0.4
0.2
0
f
$\frac{P_I}{P_O} = 0.3$
$\frac{P_I}{P_O} = 0.5$
0
0.2
0.4
0.6
0.8
$\frac{R-R_O}{R_I-R_O}$

FIG. 6

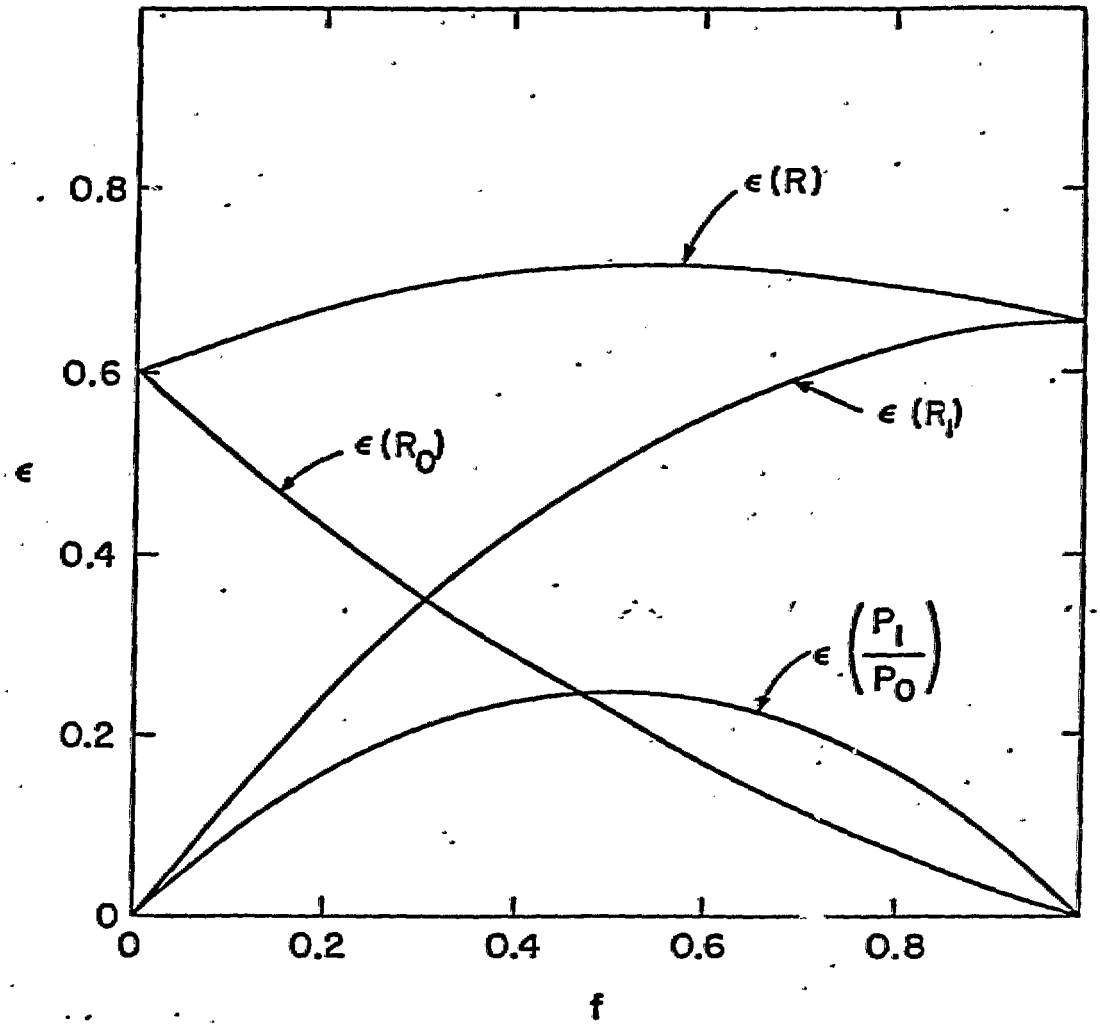
0.8
0.6
0.4
0.2
0
ε
0
0.2
0.4
0.6
0.8
f
ε (R)
ε (R_i)
ε (R_o)
ε (P_i / P_o)

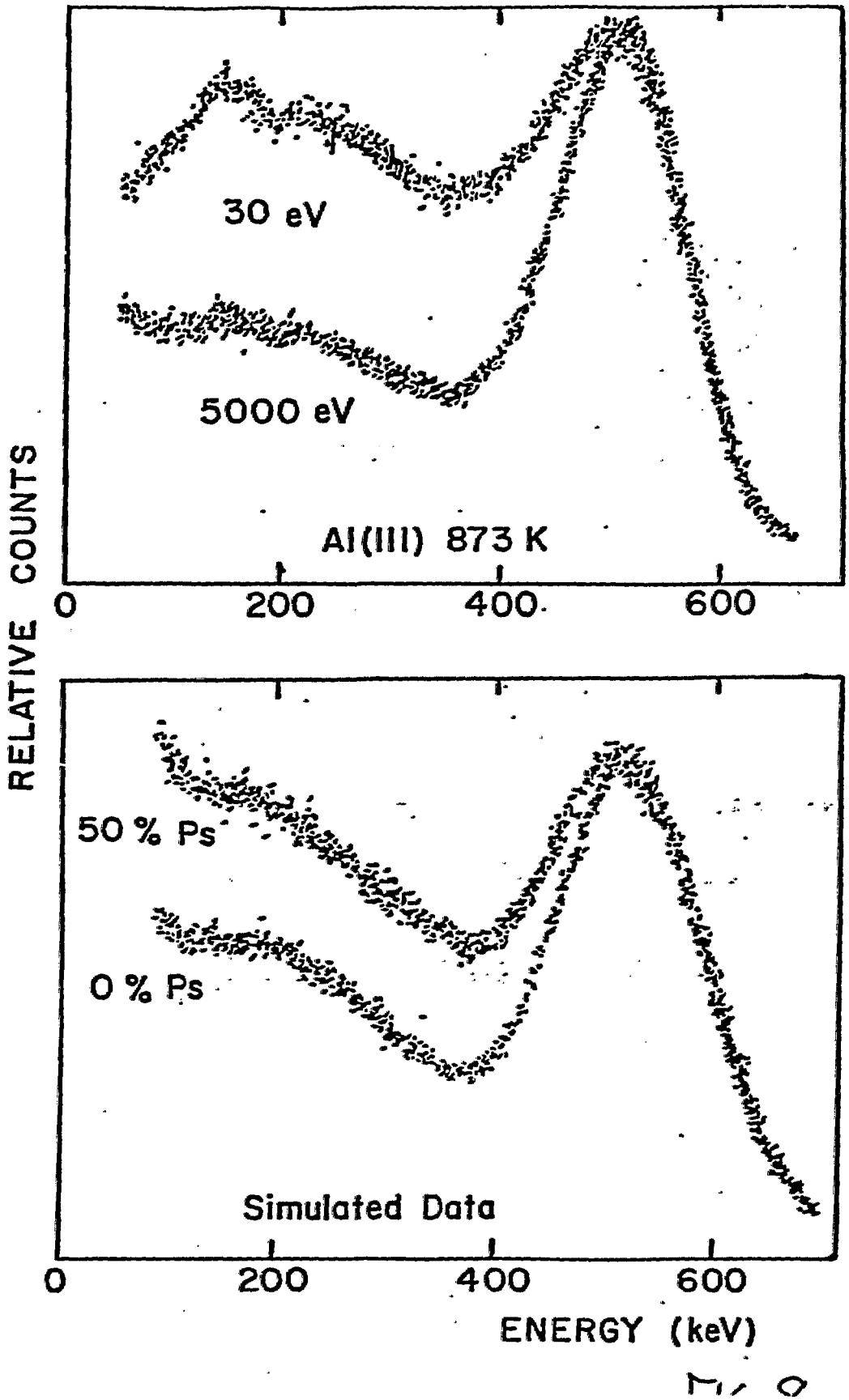
30 eV
5000 eV
Al(111) 873 K
0
200
400
600
RELATIVE COUNTS
50 % Ps
0 % Ps
Simulated Data
0
200
400
600
ENERGY (keV)

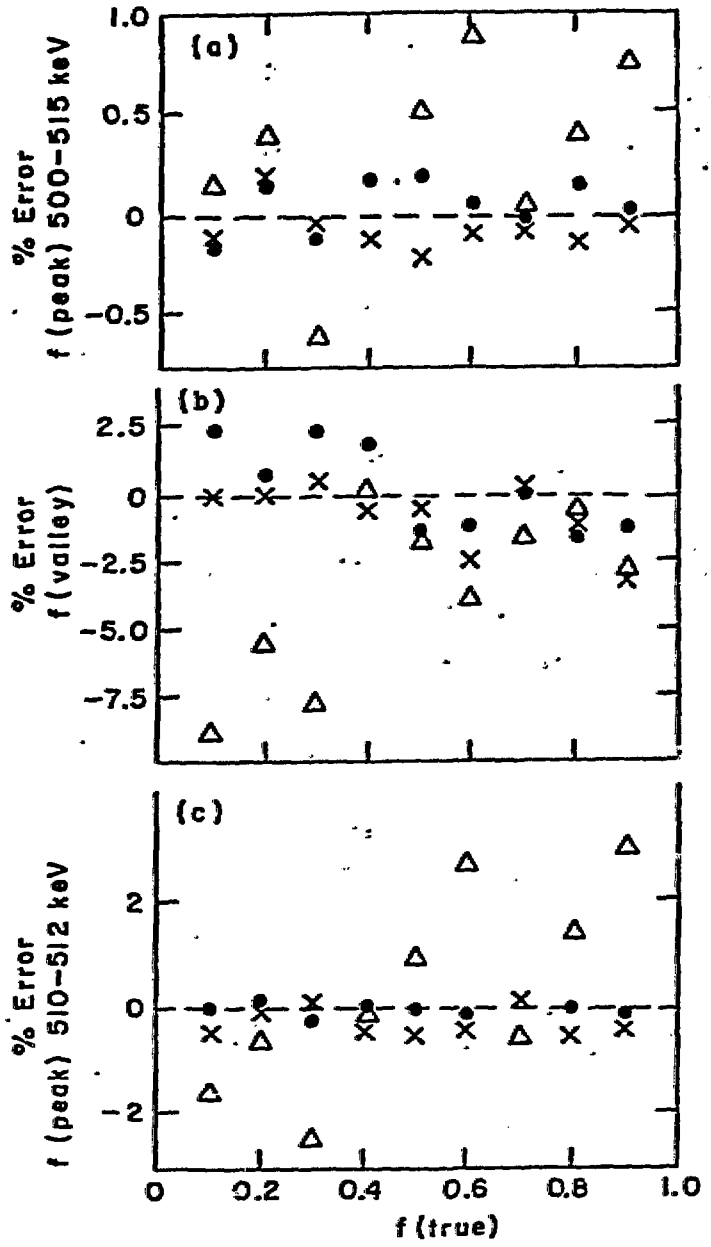
(a)
% Error
f (peak) 500–515 keV
1.0
0.5
0
−0.5
(b)
% Error
f (valley)
2.5
0
−2.5
−5.0
−7.5
(c)
% Error
f (peak) 510–512 keV
2
0
−2
0
0.2
0.4
0.6
0.8
1.0
f (true)

FIG. 9

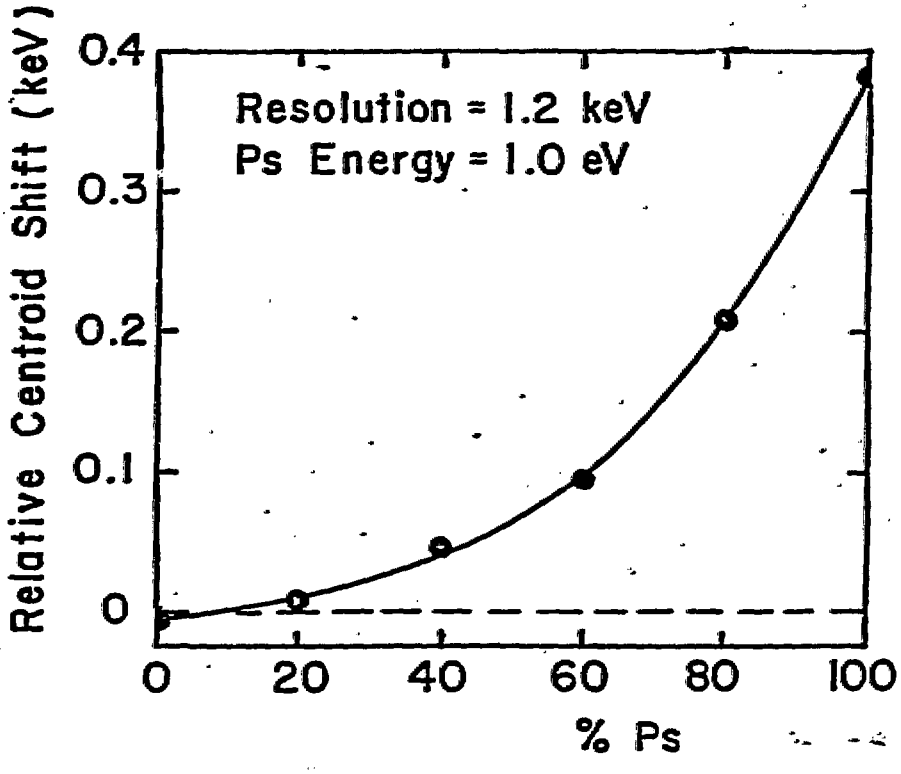
Relative Centroid Shift (keV)
0.4
0.3
0.2
0.1
0
Resolution = 1.2 keV
Ps Energy = 1.0 eV
0
20
40
60
80
100
% Ps

FIG.10

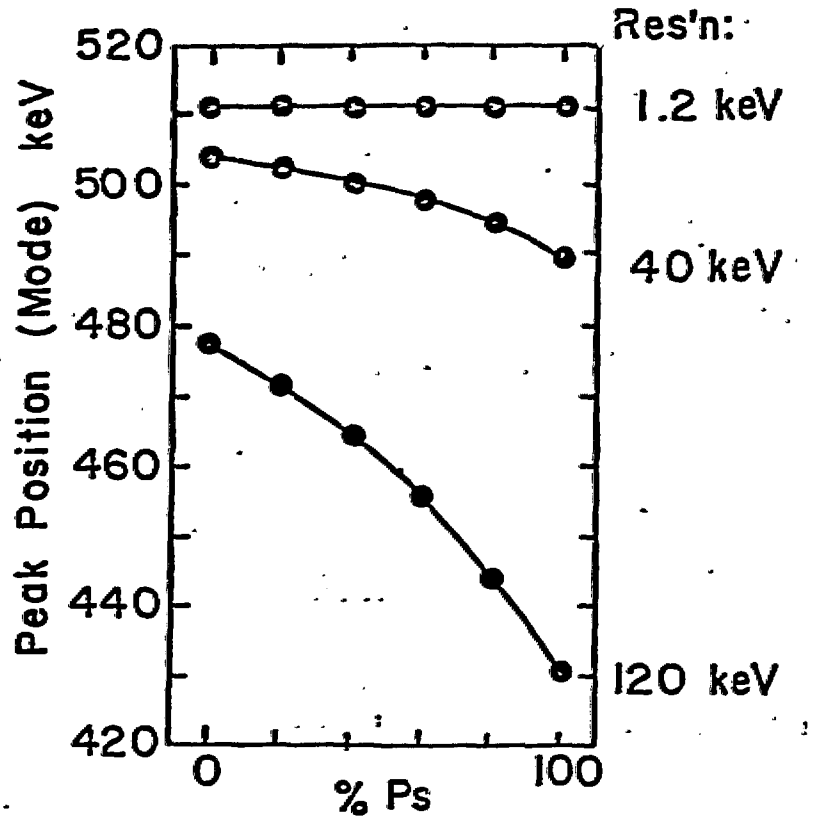
Res'n:
1.2 keV
40 keV
120 keV
520
500
480
460
440
420
Peak Position (Mode) keV
0
100
% Ps

Fig 12.